UNIVERSITÀ DI PARMA

ARCHIVIO DELLA RICERCA

University of Parma Research Repository

Detection and identification of faults in a District Heating Network

note finali coverpage

(Article begins on next page)

30 January 2025

DETECTION AND IDENTIFICATION OF
FAULTS IN A DISTRICT HEATING NETWORK

Hilal Bahlawan [a], Niccolò Ferraro [b], Agostino Gambarotta [b,c], Enzo Losi [a],

Lucrezia Manservigi [a*], Mirko Morini [b,c], Costanza Saletti [c], Pier Ruggero Spina [a], Mauro Venturini [a]

[a] Dipartimento di Ingegneria, Università degli Studi di Ferrara, via Saragat 1, Ferrara 44122, Italy,

[b] Centro Interdipartimentale per l'Energia e l'Ambiente (CIDEA), Università di Parma, Parco Area delle Scienze 181/a, Parma 43124, Italy

[c] Dipartimento di Ingegneria e Architettura, Università di Parma, Parco Area delle Scienze 181/a, Parma 43124, Italy

ABSTRACT

District Heating Networks (DHNs) are composed of numerous pipes that can be threatened by faults that affect DHN operation and management. Thus, reliable diagnostic methodologies are essential to identify DHN health state and hinder DHN malfunctioning and performance deterioration. To this purpose, a novel diagnostic approach that couples a DHN simulation model with an optimization algorithm for detecting and identifying both thermal and hydraulic faults, i.e., water leakages, anomalous heat and pressure losses, is presented in this paper. In the current paper, the novel diagnostic approach is challenged at evaluating the health state of the DHN of the campus of the University of Parma, where different faults are artificially implanted, by using a digital twin of the DHN. The faulty datasets account for both single and multiple faults, as well as different fault types and causes.

The novel diagnostic approach proves to correctly detect and identify all simulated faults, by also correctly estimating their magnitude even in the most challenging scenarios.

NOMENCLATURE

c	Specific heat capacity [J·kg^{-1}·K^{-1}]
D	Diameter [m]
f	Friction factor [-]
L	Length [m]
p	Pressure [Pa]
Q	Flow rate [kg s^{-1}]
Re	Reynolds number [-]
T	Temperature [K]
x	Health index [-]
β	Concentrated pressure losses [-]
ε	Roughness [mm]
λ	Thermal conductivity [W·m^{-1}·K^{-1}]
ρ	Density [kg m^{-3}]

Superscripts

*	Healthy condition
meas	measured

Subscripts

c	casing
down	downstream
ext	external
g	ground
in	entering
ins	insulation
int	internal
L	leakage
out	leaving
PP	power plant
Q	flow rate
r	return pipeline
s	supply pipeline
up	upstream

Acronyms

DHN	District Heating Network
EU	End-user
OF	Objective Function

1. INTRODUCTION

Problem statement and literature survey. Decarbonization of the heating sector is an effective strategy to reduce greenhouse emissions worldwide. This purpose can be achieved by exploiting District Heating Networks (DHNs) that meet end users' thermal energy demand by means of a heat carrier, e.g., water, which can be heated by fossil-free heat supplies (e.g., waste or surplus heat). Heated water subsequently flows to utilities [1] within a distribution system composed of insulated underground pipes [2]. Recent studies have investigated the benefits of coupling DHNs with additional energy systems. For example, Mateu-Royo et al. [3] documented the benefits of integrating high temperature heat pumps within DHNs. In [3], a DHN was used as a heat sink, by achieving significant performance and environmental improvements. Similarly, Balic et al. [4] coupled a combined heat and power plant with a DHN that acted as a dynamical thermal energy storage. Tveit et al. [5] presented a mixed integer nonlinear programming model employed to analyze the long-term operation of combined heat power plants in a DHN, by also considering a long-term thermal energy storage. Pardo García et al. [6] studied a district heating configuration in which photovoltaic thermal hybrid solar collectors acted as a micro-plant that

produced heat for a DHN. Ghilardi et al. [7] optimized the operation of a multi-energy system integrated with a DHN. Capone et al. [8] developed a novel approach to optimize the operation of a complex multi-energy system that also included a DHN.

The efficiency of the whole system relies on the reliability of the DHN, which can be compromised by the disruption of DHN components, e.g., sensors, pumps, equipment or heat exchangers [9, 10]. Thus, some studies, e.g., [9, 11, 12], developed novel diagnostic methodologies to identify and classify these faults. For example, Guelpa and Verda [11] proposed a diagnostic approach to automatically detect fouling in the heat exchangers located in DHN substations. The same goal was also tackled by Kim et al. [12], which used a virtual-sensor-assisted automation system suitable for buildings. Finally, Wang et al. [13] exploited a Support Vector Machine classifier to identify different types of faults.

Faults can also affect the DHN distribution system [1] which can be compromised by several malfunctions that are generally caused by both thermal and mechanical aging [14-16], as well as lack of maintenance and professional installations [16]. Therefore, reliable diagnostic methodologies are crucial to accurately evaluate the DHN health state and, if necessary, detect and identify incipient faults. Such a piece of information is extremely useful to enhance DHN performance, operation and management [17].

Pipes of DHNs are mainly affected by hydraulic faults (water leakages and increased pressure losses) and thermal faults (i.e., anomalous heat losses) [18]. Such faults reduce DHN heating quality, increase energy consumption as well as economic losses [15].

In DHNs, water leakage is the most common fault that causes approximately 33 % of DHN failures [19, 20]. According to Hallberg et al. [21], leakages are usually caused by both internal and external pipe corrosion. Internal corrosion is caused by poor water quality [1], which gradually reduces the pipe internal diameter up to its perforation. Instead, external corrosion occurs when pipes are exposed to aggressive environmental conditions due to defects in the casing. Pipe failures can also occur when welded joints weaken due to pores, in which cracks arise. In addition, leaks can also occur because of mechanical fractures and impacts due to temperature expansion, soil load and traffic load [21]. Furthermore, stress corrosion cracking and aging of pipe material [22] can also lead to pipe failures.

DHNs can be affected by anomalous pressure losses, which are provoked by the decrease of pipe internal diameter and increase of the pipe roughness. Pipe faults strictly depend on water quality. In fact, when water is oversaturated with calcium carbonate, fouling or corrosion with oxidation deposition occur within the pipe, thus leading to blockage. Fouling is the deposit of particles on the pipe internal wall, which starts as a small increase in roughness. The deposit may grow over time and eventually block a considerable portion of the pipe cross-sectional area. The same effects occur in the presence of corrosion due to oxygen dissolved in the water [23]. The consequent changes in pipe properties lead to a significant increase of pressure losses.

Dramatic consequences of pipe fouling were discussed by Walki et al. [24], which documented that 50.8 mm deposits of magnesium hydroxide were found in pipes with a 203.2 mm internal dimeter.

Finally, anomalous heat losses are usually caused by the degradation of pipe insulation. DHN pipes are composed of two insulation layers, i.e., pipe internal insulation and pipe external casing, that are usually made of rock wool and polyethylene [25], respectively. Each pipe insulation layer deteriorates over time because, during operating conditions, pipes are affected by temperature variations due to fluctuations in customer demands, pipe-soil interactions or atmospheric conditions. The resulting mechanical and thermal loads often lead to damage and ageing [26]. In such conditions, the performance of the pipe insulation layer decreases, leading to a local increase in the thermal conductivity and, thus, higher thermal energy losses [19]. Consequences of insulation deterioration may also be dramatic, as experienced in a Swedish DHN, where 10 % of thermal energy was lost because of insulation failures [14].

Faults of the insulation layers affect thermal heat losses in different ways. Faults that impact the external casing are extremely dangerous because moisture enters the pipe, by leading to two negative consequences. First, moisture dampens pipe insulation, by

increasing its thermal conductivity λ [21]. As a consequence, pipe thermal resistance decreases, by increasing heat losses, accordingly. For example, if the moisture content is equal to 13.6 %, the thermal conductivity of the rock wool is up to four times higher than its value at dry condition [27]. Secondly, moisture corrodes pipes [21], which weaken and, subsequently, break.

As outlined in the literature, only few studies addressed the development of accurate methodologies for fault detection in DHNs. Leakages in DHNs are currently detected by monitoring the ground moisture level [21]. However, DHN diagnosis may provide misleading results due to the influence of groundwater and rainwater [21]. Leakages may also be detected by observing the make-up flow rate [15, 28] that, at healthy conditions, is usually lower than 1 % of the total flow rate [15]. Thus, a fault may occur when the rate of the lost water is higher than 1 % of the total flow rate [15]. In addition, the pressure gradient method may be a viable physics-based diagnostic approach since it exploits the propagation of pressure waves within the DHN [28] to detect the actual point at which leakage takes place [29]. Kaliatka and Valincius [30] developed a general methodology aimed at identifying pipe break location, by considering pressure decrease and propagation. Alternatively, leakages may be detected by means of data-driven models, which can be quite easily developed, but their reliability strictly depends on data availability and quality [29]. For instance, both machine learning approaches (e.g., the least-squares support vector machine classifier) and artificial intelligence tools (e.g., multi-layer perceptron neural network, convolutional neural network) [15, 18] can be used. According to Zhou et al. [29], data-driven modeling approaches also comprise the resistance and impedance methods, which detect the failure point by monitoring the voltage or the pulse signal between two signal wires inserted within pipe insulation [29].

Finally, the "unmanned airborne infrared thermography" method is a viable alternative to both physics-based and data-driven approaches, since pipe failure is detected by using thermal images that reveal the increase in the ground temperature due to hot water leaks [29] by means of handheld thermal cameras. However, fault detection may be challenged when a fault occurs in large-scale and complex DHNs, especially when they are placed in areas that are difficult to access. To this purpose, Zhong et al. [31] presented a saliency analysis method for detecting water leakages, by using remotely sensed infrared imagery, visible imagery and geographic information systems data.

For evaluating pipe pressure losses, Kane and Rolle [32] developed a novel diagnostic approach that grouped several substations, i.e., end-users, and pipes into clusters.

Anomalous heat losses can be detected by means of both data-driven models and physics-based approaches. For example, Chicherin et al. [33] exploited a data-driven approach to investigate the relationship between different states of pipe insulation and heat losses. Instead, a non-destructive method was developed by Lidén et al. [34] for assessing the thermal conductivity of the insulation of an aged pipe. To this purpose, drainage valve measurements were coupled with a numerical model that calculated the temperature decline during DHN shutdown. Instead, the model proposed by Fang and Lahdelma [35] detected faults affecting DHNs by calculating mass flow rates, temperatures and heat losses. Instead, Wang et al. [17] detected heat losses by exploiting a genetic algorithm that compared the measured and calculated DHN variables, i.e., flow rate, pressure and temperature.

Paper's novelty and contribution. The current paper is aimed at developing a novel diagnostic approach that evaluates DHN health state by detecting and identifying faults that affect DHN pipes. Detection allows the localization of the faulty pipe, while identification aims at assessing fault type and magnitude. The novel diagnostic approach is validated by using several datasets generated by a *digital twin* of the DHN of the campus of the University of Parma, which is used as the case study. In fact, the common practice consists of preliminarily testing a novel approach by means of simulated data.

With respect to state-of-the-art literature, the novelty of this paper can be summarized as follows:

- development of a novel diagnostic approach that provides the "health indices" for all DHN pipes, by allowing an effective evaluation of DHN health state;

- combined detection and identification of three fault types, i.e., water leakages, anomalous heat losses and anomalous pressure losses. This multiple capability represents a novelty since the common practice consists of detecting faults one by one. In addition, the detection of anomalous pressure losses has been usually neglected in the literature;

- detection and identification of both single and multiple faults. In the current paper, a single fault occurs when only one pipe is faulty and the fault cause is unique. Conversely, a multiple fault accounts for multiple causes. It has to be highlighted that multiple faults have been rarely investigated in the literature;

- validation of the proposed diagnostic approach by considering different and heterogenous faulty scenarios. In fact, the diagnostic approach is checked against both single and multiple faults, by accounting for different fault types, causes and magnitudes.

The paper is structured as follows. First, the diagnostic approach is developed, by highlighting its basics and defining pipe health indices (Section 2). The case study is described (Section 3), together with the *digital twin* of the DHN and the considered faulty datasets; the diagnosis of the faulty datasets is subsequently reported (Section 4), as well as a thorough discussion about methodology capability and paper's achievements. Finally, the Conclusions are drawn (Section 5).

2. DIAGNOSTIC APPROACH

To evaluate the health state of a DHN, this paper adapts the theoretical approach developed by Bettocchi and Spina [36] and subsequently successfully employed for gas turbine diagnostics in [37, 38, 39].

The novel diagnostic approach is aimed at detecting and identifying water leakages, anomalous heat losses and anomalous pressure losses that affect DHN pipes. To this purpose, the novel diagnostic approach labels each pipe of the DHN by means of three health indices, i.e., x_Q, x_{Rth} and x_{Rp}, that comprehensively assess the health state of the pipe. The health index x_Q refers to leakages along pipes, while x_{Rth} and x_{Rp} identify anomalous heat and pressure losses, respectively. Thus, a health index is equal to one at healthy conditions, whereas it is lower than one when a fault occurs; the lower the health index, the more severe the fault.

As depicted in Fig. 1, the diagnosis of the DHN is performed by developing a DHN model that calculates mass flow rate, temperature and pressure in all pipes.
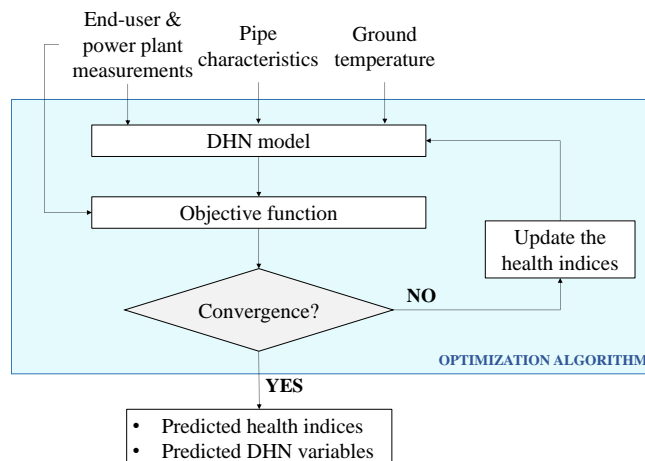
To this purpose, an optimization algorithm adjusts all health indices until the objective function converges.

It has to be observed that the diagnostic approach allows DHN diagnosis under steady-state condition and thus it is independent of system operating condition. In addition, since the diagnostic approach exploits balances, the diagnosis of the system holds independently of DHN layout, number of power plants and end-users.

The DHN model, its inputs and the outputs are briefly described in the following; additional information about the DHN model is reported in Manservigi et al. [40].

DHN model. The DHN model is aimed at calculating the flow rate of each pipe, as well as the temperature and pressure at each node. In this paper, it is assumed that four different node types can be encountered, i.e., the thermal power plant, splitting junction nodes, mixing junction nodes and end-user (EU) nodes. The heat transfer fluid (i.e., water) is warmed in the thermal power station and distributed by means of the supply pipeline. Thanks to splitting junction nodes, warm water is split into several branching pipelines towards end-user nodes, which correspond to the heat exchangers of the building substations. Then, return water flows exiting the various substations are mixed within mixing junction nodes and led back to the thermal power station through the main return pipeline.

The mass flow rate (Q) flowing through each pipe is calculated by accounting for the contribution of each Q that enters and leaves a node. To this purpose, a set of N_n equations as the one reported in Eq. (1) is solved.

$$\sum x_Q Q_{in} - \sum Q_{out} - \sum Q_{EU} = 0 \tag{1}$$

In Eq. (1), $x_Q \cdot Q_{in}$ is the actual flow rate entering a node, while Q_{out} and Q_{EU} are the flow rates that leave that node and subsequently flow towards a splitting (or mixing) junction or an end-user node, respectively.

In the supply pipeline, the temperature of each node is calculated by using the thermal power balance solved under steady-state conditions and by assuming that the specific heat c is constant (see Eq. (2)). The temperature of each node is calculated by considering three thermal power contributions along the entire pipe length, as shown in Fig. 2.
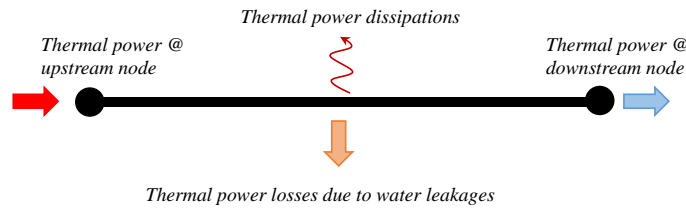

Figure 2 – Thermal power contributions considered for calculating the temperature of DHN nodes.

The first contribution corresponds to the thermal power that enters a pipe, which depends on the temperature of the upstream node T_{up} of the pipe under analysis. The thermal power that leaves the pipe is the second term of Eq. (2), which depends on the temperature of the downstream node T_{down}. Finally, thermal power losses include both the thermal losses caused by the water leakages as well as the dissipations through pipe walls. The thermal power lost due to water leakages depends on the amount of water that leaks, i.e. $(1 - x_Q) \cdot Q$.

In this paper, such a term depends on both T_{up} and T_{down}. Finally, thermal dissipations through pipe walls are calculated by considering the ground temperature T_g and the thermal resistance R_{th}.

$$cQT_{up} - cx_Q QT_{down} - c(1-x_Q)Q\left(\frac{T_{up}+T_{down}}{2}\right) - \frac{1}{R_{th}}\left(\frac{T_{up}+T_{down}}{2} - T_g\right) = 0 \tag{2}$$

As in [41], thermal resistance R_{th} accounts for internal convection and conduction of each pipe layer, i.e., steel pipe, insulation and external casing (Eq. (3)).

$$R_{th} = x_{Rth}\left[\frac{1}{\pi L D_{int,p} k_{conv,int}} + \frac{1}{2\pi L\lambda_p}\ln\left(\frac{D_{ext}}{D_{int}}\right) + \frac{1}{2\pi L\lambda_{ins}}\ln\left(\frac{D_{ins}}{D_{ext}}\right) + \frac{1}{2\pi L\lambda_c}\ln\left(\frac{D_c}{D_{ins}}\right)\right] \tag{3}$$

To calculate the heat transfer coefficient, i.e. $k_{conv,int}$, the Nusselt number and the friction factor are calculated by using the temperature of the upstream node.

In the supply pipelines, the temperature of each node of the DHN is calculated starting by the pipe that is fed by the power plant, of which the temperature is usually known. Thus, Eq. (2) allows the calculation of the only unknown variable, i.e., T_{down}, and the temperature of the remaining nodes is sequentially calculated.

In the return pipeline, the temperature of each *end-user* node T_{EU} is calculated by subtracting the temperature drop (ΔT) caused by the heat exchanger from the temperature of the end-user node in the supply pipeline.

Instead, the temperature of both *mixing junction nodes* and *thermal power plant* are calculated by assuming adiabatic mixing.

Finally, the pressure of each node is calculated by considering the entire pipe length, by solving a set of N_P equations as the one reported in Eq. (4)

$$-p_{up} + p_{down} + \Delta p = 0 \tag{4}$$

With respect to the flow rate direction, the variables p_{up} and p_{down} represent the pressure at the upstream and downstream node of a pipe, respectively. Pressure loss through a pipe, i.e., Δp, is calculated as in Eq. (5):

$$\Delta p = R_p Q^2 \tag{5}$$

The coefficient R_p accounts for both concentrated and distributed pressure losses, which depend on the pipe internal diameter D_{int}, the length of the pipe L, the coefficient of concentrated losses β, the fluid density and the friction factor as follows

$$R_p = \frac{1}{x_{Rp}}\left[\frac{8}{\rho(\bar{T})\pi^2 D_{int}^4}\left(f(\bar{T})\frac{L}{D_{int}} + \beta\right)\right] \tag{6}$$

As in [41], both fluid density and friction factor depend on the mean temperature between the upstream and downstream nodes of each pipe under analysis.

Inputs, outputs and objective function. The inputs of the diagnostic approach are distinguished between independent and dependent variables, which are used in different ways.

The *independent variables* feed the DHN model to calculate the mass flow rates, temperatures and pressures. To this aim, some end-user measurements have to be provided, as the flow rate entering each end-user heat exchanger Q_{EU} and the water pressure and temperature drops through the heat exchangers (see Table 1).

<div align="center">

Table 1 – Inputs and outputs of the diagnostic approach

</div>

	Description	Variables	
		Independent variables	
Inputs	End-user measurements	$Q_{EU,i}^{meas}$, $\Delta T_{EU,i}^{meas}$, $\Delta p_{EU,i}^{meas}$	$i = 1, \dots N_{EU}$
	Power plant measurements	$p_{PP,i,s}^{meas}$, $T_{PP,i,s}^{meas}$, $p_{PP,i,r}^{meas}$	$i = 1, \dots N_{PP}$
	Pipe characteristics	L_i, $D_{int,i}$, $D_{ext,i}$, $D_{ins,i}$, $D_{c,i}$, β_i, $\lambda_{P,i}$, $\lambda_{ins,i}$, $\lambda_{c,i}$, ε_i	$i = 1, \dots N_P$
	Ground temperature	T_g	
		Dependent variables	
	End-user measurements	$T_{EU,i,s}^{meas}$, $T_{EU,i,r}^{meas}$, $p_{EU,i,s}^{meas}$, $p_{EU,i,r}^{meas}$	$i = 1, \dots N_{EU}$
	Power plant measurements	$Q_{PP,i,s}^{meas}$, $Q_{PP,i,r}^{meas}$, $T_{PP,i,r}^{meas}$	$i = 1, \dots N_{PP}$
Outputs		*Predicted health indices*	
	Leakages	$x_{Q,i,s}$, $x_{Q,i,r}$	$i = 1, \dots N_P$
	Thermal losses	$x_{Rth,i,s}$, $x_{Rth,i,r}$,	$i = 1, \dots N_P$
	Pressure losses	$x_{Rp,i,s}$, $x_{Rp,i,r}$	$i = 1, \dots N_P$
		Predicted DHN variables	
	Calculated dependent variables	Q_i, T_i, p_i	$i = 1, \dots N_n$

In addition, the pressure at the power plant has to be known, both in the supply and return pipelines, as well as the temperature at the power plant in the supply pipeline.

Temperature and pressure of each node are influenced by pipe characteristics. Thus, both geometrical (e.g., D) and thermal (i.e., λ) characteristics of each layer of the pipe (pipe wall, insulation and external casing) have to be provided. Finally, as highlighted in Eq. (2), the ground temperature T_g is required to evaluate heat losses.

The *dependent variables* (Table 1) feed the objective function F_{ob} reported in Eq. (7) that compares the measured physical quantities to the same values calculated by the DHN model. To this purpose, temperature and pressure of each end-user, as well as themass flow rate and temperature of the power plant, have to be known.

$$F_{ob} = \left(\frac{Q_{PP}^{meas} - Q_{PP}}{Q_{PP}^{meas}}\right)_s^2 + \left(\frac{Q_{PP}^{meas} - Q_{PP}}{Q_{PP}^{meas}}\right)_r^2 + \left(\frac{T_{PP}^{meas} - T_{PP}}{T_{PP}^{meas}}\right)_r^2 + \sum_i^{N_{EU}} \left(\frac{T_{EU,i}^{meas} - T_{EU,i}}{T_{EU,i}^{meas}}\right)_s^2 + \left(\frac{T_{EU,i}^{meas} - T_{EU,i}}{T_{EU,i}^{meas}}\right)_r^2 + \left(\frac{p_{EU,i}^{meas} - p_{EU,i}}{p_{EU,i}^{meas}}\right)_s^2 + \left(\frac{p_{EU,i}^{meas} - p_{EU,i}}{p_{EU,i}^{meas}}\right)_r^2 \qquad (7)$$

In this paper, it is assumed that:

- each power plant of the DHN is equipped with one flow rate meter, one temperature sensor and one pressure sensor, in both the supply and return pipelines (see Fig. 3(a));
- each end-user, in the supply pipeline, is equipped with one flow rate meter, one temperature sensor and pressure sensor, which have to be installed upstream of the by-pass valve (see Fig. 3(b)), while in the return pipeline, one temperature sensor and one pressure sensor are installed downstream of the by-pass valve (see Fig. 3(b)).
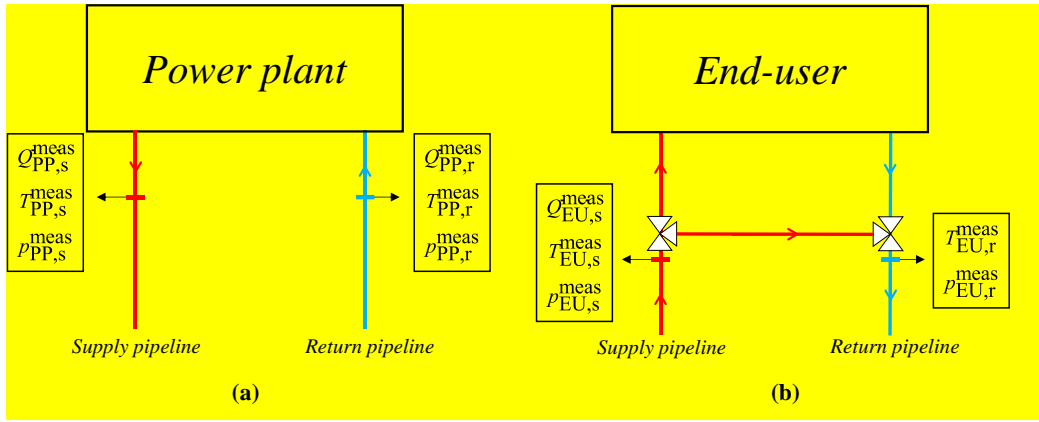

Figure 3 – Sensors (location, number and type) required to apply the diagnostic approach

The outputs of the diagnostic approach are the six health indices of each pipe, i.e., $x_{Q,s}$, $x_{Rth,s}$, $x_{Rp,s}$, $x_{Q,r}$, $x_{Rth,r}$, $x_{Rp,r}$, in both the supply and return pipelines, as well as all the calculated DHN variables (i.e., mass flow rate, temperature and pressure). These values are obtained by using an optimization algorithm that minimizes the objective function by updating the health indices until the F_{ob} converges.

3. CASE STUDY

District heating network. The proposed diagnostic approach is checked to detect and identify faults hypothetically affecting the DHN of the campus of the University of Parma (Italy). The DHN has four main branches, supplied by five natural gas boilers. The simulated portion of the system is the "Nuova Sud" branch of the network (Fig. 4), which distributes heat to twelve connected end-users, i.e., departments, laboratories, classrooms and cafeterias [42].
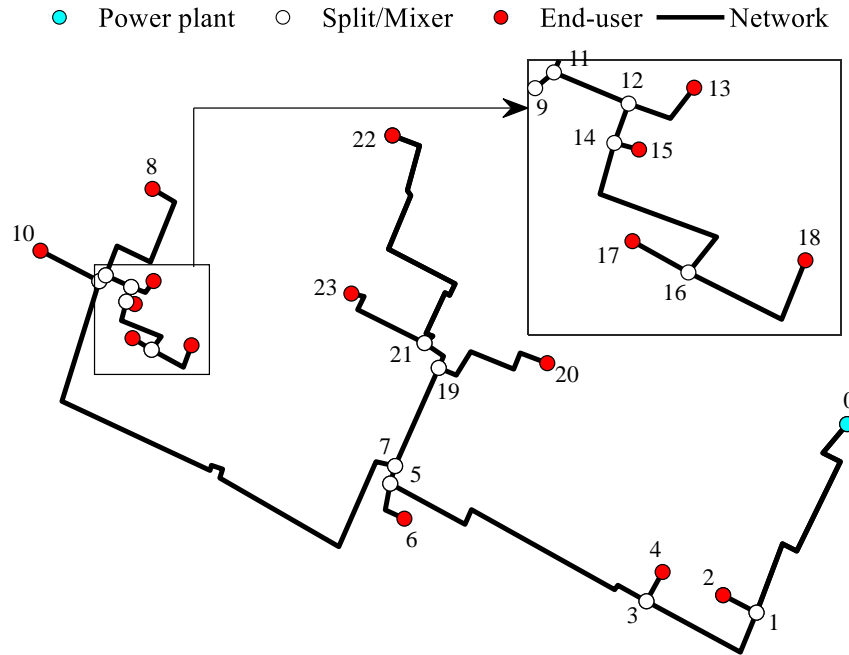
Figure 4 – Scheme of the considered portion of the DHN of the campus of the University of Parma

The heat transfer fluid (i.e., water) is warmed in the thermal power plant and distributed by means of the main supply pipeline towards the building substation heat exchangers. The water mass flow rate entering each user substation (end-user) can be recirculated by means of a three-port valve, in order to regulate the heat supplied to the building and keep indoor comfort requirements. Then, the return water flows from the various substations and is led back to the thermal power station through the main return pipeline.

By considering both the supply and return pipelines, the DHN includes forty-six pipes in total and is approximately 4 km long. Fig. 4 depicts the supply pipeline of the considered DHN. In addition, forty-eight nodes in total are considered, corresponding to one thermal power plant, eleven splitting and mixing junction nodes and twelve end-user nodes, for both the supply and the return pipeline. Since the DHN of the campus of the University of Parma comprises one power plant and twelve end-users, as shown in Fig. 4, sixty-six measurement devices, i.e., fourteen flow meters, twenty-six temperature sensors and twenty-six pressure sensors, are required to be installed as in Fig. 3(a) and (b).

Given that (i) the health state of each pipe is described by means of three health indices, (ii) the DHN diagnosis is performed on both the supply and return pipelines and (iii) both the supply and return pipelines include twenty-three pipes, 138 health indices in total have to be predicted by the diagnostic methodology.

Digital twin of the DHN. To check and validate the diagnostic model developed in this paper, end-user, power plant measurements and the ground temperature (see Fig. 1 and Table 1) were generated by means of the model developed in [41]. As demonstrated in [42], such a model provides a detailed and feasible representation of the behavior of the DHN of the campus of the University of Parma. Thus, the model can be used as a *digital twin* of the DHN investigated in this paper. The exploitation of such a digital twin relies on the fact that the validation of a diagnostic tool is generally hindered by the lack of both complex experimental laboratory-scale setups and large-scale labeled datasets (i.e., both the fault and its time of occurrence must be known) [43].

The *digital twin* was built by means of a dedicated library, developed in the MATLAB®/Simulink® environment, that simulates energy conversion devices, distribution systems and end-users. The model considers both the hydraulic and thermal domains to describe the evolution of the main thermodynamic parameters of the heat transfer fluid in each section of the network. To this purpose, the conservation equations of mass, momentum and energy in differential form are used. Such a high level of detail allows accurate monitoring of mass flow rates, temperatures and pressures throughout the system with a user-defined time granularity.

In the model developed in [41], the distribution system comprises pipelines and junction nodes. The pipe model can be discretized in the axial direction by assembling in sequence several pipe segments, including both thermal and fluid dynamics of water. On the other hand, junction node models allow mixing/splitting flows from/to several different pipe segments, to represent branching pipelines and collectors. The junction dynamic model calculates the local temperature and pressure based on inlet and outlet flows by means of energy balance and continuity equations. The end-user block includes a heat exchanger representing the heat transfer between the distribution water and the building itself.

The inputs of the model can be provided by experimental measurements or building simulation software. The model calculates all DHN variables as well as the ground temperature variations for a given geographical area.

Further details about model structure and equations are reported in [41].

Implanted faults. The digital twin was employed to generate twenty-three datasets, each of them comprising ten consecutive days of operation, to mimic DHN operation under both transient and steady-state conditions.

One of these datasets reproduces DHN healthy condition, which considers that pipes are made of steel ($\lambda^*_P = 57$ W·m^{-1}·K^{-1}) and are thermally insulated by means of a rock-wool layer ($\lambda^*_{ins} = 0.04$ W·m^{-1}·K^{-1}) and an external casing ($\lambda^*_c = 1$ W·m^{-1}·K^{-1}). Pipe roughness ε^* is equal to 0.1 mm. Figure 5 shows the trend of mass flow rate, pressure and temperature of the power plant in the supply pipeline during ten days of operation under healthy conditions.
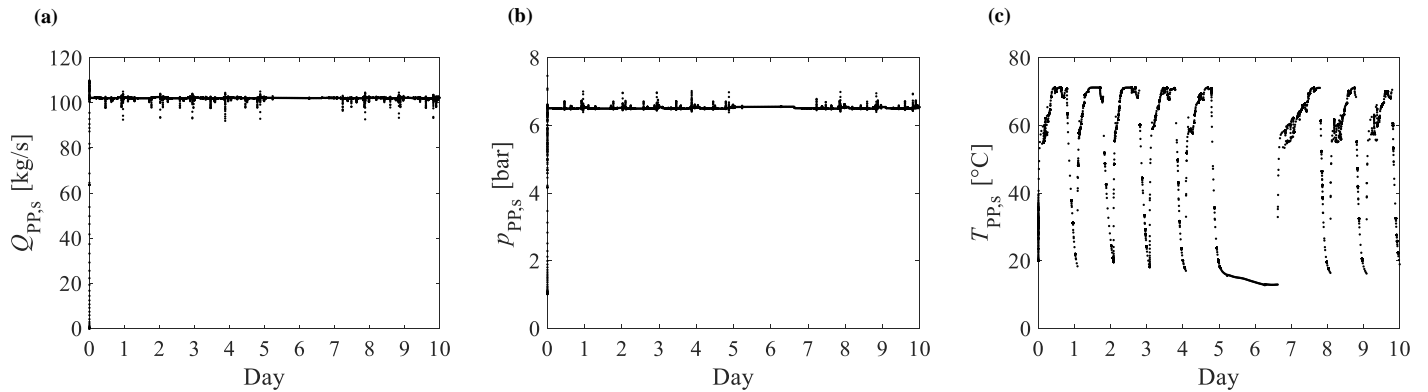

Figure 5 – Mass flow rate (a), pressure (b) and temperature (c) of the power plant in the supply pipeline during ten days of operation under healthy conditions (values simulated by the *digital twin* of the DHN)

The remaining twenty-two datasets were generated by considering the same boundary conditions (e.g., ground temperature and thermal energy demand of the end-users), but one or more faults were implanted by modifying pipe characteristics, i.e., ε and λ_{ins}, D_{int}. The digital twin of the DHN simulated the anomalous heat losses, anomalous pressure losses and water leakages as follows.

The anomalous heat losses were modeled by increasing the thermal conductivity of the insulation layer (see Table 2) with respect to the healthy condition. To mimic anomalous pressure losses, the pipe roughness or internal diameter of the faulty pipe were varied

because of pipe fouling or corrosion. Faults that cause anomalous heat and pressure losses can affect the entire length or a portion of the pipe.

Table 2 - Cause, effect and locations of the faults simulated by means of the digital twin.

Fault cause	Fault effect	Fault location	Change in the digital twin
Degradation of pipe insulation	Anomalous heat losses	Pipe segment or entire pipe	Increase in insulation thermal conductivity
Pipe fouling or corrosion	Anomalous pressure losses	Pipe segment or entire pipe	Increase in pipe roughness
		Pipe segment or entire pipe	Reduction in pipe internal diameter
Pipe perforation	Leakage	Node	Additional outlet water flow from an already existing junction node
		Pipe	Additional junction node with outlet water flow between two pipe segments

Finally, two types of water leakage with different fault location were simulated. First, leakages occurring along the pipe were accounted for. The digital twin modeled this faulty scenario by adding one intermediate splitting junction node, from which the water leakage leaves the pipe. In such a way, in the faulty pipe, the mass flow rate in the upstream node is higher than the mass flow rate in the downstream node, according to Eq. (1). In addition, the novel diagnostic approach was also checked to detect water leakages due to a faulty splitting or mixing junction node. The digital twin modeled this fault by accounting for an additional Q_{out} (see Eq. (1))) in the faulty node. The diagnosis of this faulty scenario is extremely challenging for the novel diagnostic approach, since, by definition, the health index x_Q accounts for water lost in a pipe, not in a node, as mentioned in the discussion about Eq. (1).

As an anticipation of the results, it can be stated that the novel diagnostic approach accurately detected and identified all the twenty-two faults simulated by the digital twin, by also evaluating the actual fault magnitude. However, the results and the analyses presented in this paper focus on seven out of twenty-two faulty datasets, namely Fault #1 through #7 (see Table 3). The seven faulty datasets account for all fault causes and different fault locations (e.g., the entire length of the pipe or a fraction of the pipe), by including both single (Fault #1 through #5) and multiple (Fault #6 and #7) faults. Despite single faults are more likely than multiple faults, Fault #6 and #7 are also discussed to thoroughly evaluate the capability of the novel diagnostic approach even in the most challenging scenarios.

For the sake of clarity, each pipe is labeled according to its upstream and downstream nodes.

The anomalous heat losses of the Fault #1 (see Table 3) were caused by an increase of λ_{ins} along the entire length of the faulty pipe, i.e., pipe 19-20. Instead, the anomalous pressure losses experienced by the pipe delimited by the nodes 19 and 20 were caused by an increase in the pipe roughness that, in the faulty scenario "Fault #2", is equal to 1 mm, i.e., ten-times higher than under healthy condition. Instead, the anomalous pressure losses simulated in Fault #3 occurred because the internal diameter of pipe 12-14 was halved with respect to the healthy conditions along 10% of pipe length. Fault #4 and #5 differ from each other in the location of the leakage point, which was located within the pipe or at its downstream node, respectively. In both cases, the lost water was approximately 2.0 % of the water that leaves the thermal power plant.

Fault #6 included both anomalous heat and pressure losses caused by the increase of λ_{ins} and the decrease of the internal diameter.

The anomalous pressure losses that characterize Fault #7 were caused by both an increase in the pipe roughness and a decrease in the pipe internal diameter of the pipe 12-14. As in Fault #2 and #3, pipe roughness is ten times the value under healthy condition, while the internal diameter was halved. For both Fault #6 and #7, the pipe internal diameter halved along 10% of pipe length.

Finally, it is worth highlighting the influence of the accuracy of temperature measurements. In fact, in the interval of interest, i.e., 30 °C – 90 °C, the uncertainty of temperature sensors employed in a DHN may be in the range from 0.45 °C to 0.75 °C [44]. Thus, the faults that affect pipe insulation were selected so that the temperature variation due to a fault is higher than 1 °C.

Table 3 - Implanted faults analyzed in this paper

Fault no.	Effect of the fault	Faulty pipe	Fault location	Faulty parameter	Healthy parameter
#1	Anomalous heat losses	19-20	Entire pipe	$\lambda_{ins} = 2.00$ W m^{-1} K^{-1}	$\lambda^*_{ins} = 0.04$ W m^{-1} K^{-1}
#2	Anomalous pressure losses	19-20	Entire pipe	$\varepsilon = 1.00$ mm	$\varepsilon^* = 0.1$ mm
#3	Anomalous pressure losses	12-14	10% of pipe length	$D_{int} = 0.0625$ m	$D^*_{int} = 0.1250$ m
#4	Water leakages	11-12	Pipe	$Q_L = 2$ kg s^{-1}	No leakage
#5	Water leakages	12	Node	$Q_L = 2$ kg s^{-1}	No leakage
#6	Anomalous heat losses / Anomalous pressure losses	12-14	Entire pipe / 10% of pipe length	$\lambda_{ins} = 20.00$ W m^{-1} K^{-1} / $D_{int} = 0.0625$ m	$\lambda^*_{ins} = 0.04$ W m^{-1} K^{-1} / $D^*_{int} = 0.1250$ m
#7	Anomalous pressure losses	12-14	Entire pipe / 10% of pipe length	$\varepsilon = 1.0$ mm / $D_{int} = 0.0625$ m	$\varepsilon^* = 0.1$ mm / $D^*_{int} = 0.1250$ m

4. RESULTS

The capability of the diagnostic approach to evaluate the health state of the DHN of the campus of the University of Parma, whose measured variables were generated by the *digital twin* described in Section 3, is investigated in this Section.

Since the diagnostic approach is used under steady-state conditions, the DHN diagnosis is performed by considering a single operating condition at which all DHN variables simulated by the digital twin exhibit a steady-state behavior in all nodes. To this purpose, a moving window of 60 minutes was considered, by calculating the mean value and standard deviation of each physical quantity. A steady-state time point is identified when the coefficient of variation, i.e., the ratio between the standard deviation and the mean value, of all physical quantities at all DHN nodes is lower than 10^{-6}.

In line with the procedure discussed in Section 2, the diagnostic approach identifies pipe health indices by exploiting an optimization algorithm based on a gradient-based method that is available in the Matlab® environment [45]. In fact, based on a specific analysis conducted by the authors, such optimization algorithm proved more accurate than alternative options (e.g., genetic algorithm), by also significantly reducing the computational time, which is in the range from 30 s to 2 mins for the system layout and faults considered in this paper. Such features are crucial to promptly identify possible losses and take proper actions.

In the optimization procedure, the lower and upper bounds of the search space of health indices were set equal to 10^{-3} (i.e., 99.9% decrease) and 1.0 (healthy condition), respectively. The starting value for the optimization was set equal to 1.0: in this way, at the first guess, the system is assumed healthy. The optimization procedure stops when the variation of the objective function is lower than 10^{-9}. The diagnostic approach is challenged to detect and identify the faulty pipe and the type of fault, as well as its magnitude. To this purpose, the DHN measurable variables generated by the digital twin) are compared to the corresponding predicted measurable variables calculated by the diagnostic approach.

First, each faulty scenario was compared to the healthy condition to evaluate the effects of faults on the DHN variables. This analysis is summarized by means of Figs. 6, 8, 10, 12, 17 and 19, which compare each physical quantity under the faulty scenario (Y in Eq. (8)) to the same physical quantity under healthy condition (Y^* in Eq. (8)).

$$\delta Y = \frac{Y - Y^*}{Y^*} \quad , Y = Q, T, p \tag{8}$$

The goal of this analysis is out to display the pieces of information available to the DHN monitoring system. As shown in Figs. 6, 8, 10, 12, 17 and 19, the effect of faults is usually almost uniformly spread over the measurable variables, according to DHN topology. Thus, the diagnosis of DHN health state would be impossible by just monitoring the measurable variables. Instead, as shown in the following, the health indices provide univocal pieces of information about fault type, localization and magnitude.

Secondly, the expected and predicted health indices are documented. It has to be highlighted that the expected x_{Rth} and x_{Rp} are calculated by comparing R_{th} and R_p of the faulty scenarios simulated by the digital twin to the same values at healthy conditions. In addition, for a given leaking pipe, the expected x_Q is calculated by dividing the amount of water that enters its downstream node by the amount of water that feeds its upstream node.

The capability of the diagnostic approach to calculate DHN variables is also assessed. To this purpose, the expected and predicted R_{th} and R_p of the faulty pipes are evaluated, as well as the expected and predicted temperature and pressure drop from the healthy condition (T^*, p^*) to the faulty scenario (T, p). In case of leakage, the rate of lost water is discussed.

The prediction error on each DHN variable is also reported, both in absolute (difference between expected and predicted Q, T and p) and relative (ratio of the absolute prediction error to the expected value) terms. It should be noted that the relative temperature error is calculated by expressing temperature values in degrees Celsius.

The diagnosis of Fault #1 through #7 performed by the diagnostic approach is shown in Figs. 7, 9, 11, 13, 15, 18, 20. For each faulty dataset, a heatmap chart is reported, where the color depends on the predicted health index. For the sake of clarity, the predicted $x_{Rth,s}$ and $x_{Rth,r}$ are shown in a logarithmic scale. In Figs. 7, 9, 11, 13, 18, 20, the "X" symbol highlights the actual faulty pipe and fault type, i.e., the response that the diagnostic approach is expected to target. In Fig. 15, the "X" symbol is not reported because water leakage occurs at a node.

The diagnostic approach was preliminarily validated under healthy conditions by using a healthy dataset whose expected health indices were equal to one. The diagnostic approach proved very accurate, since all the predicted health indices were always higher than 0.995.

4.1 Diagnosis of single faults

Fault #1: anomalous heat losses within pipe 19-20. In the first dataset, pipe 19-20 is affected by anomalous heat losses caused by the increase of the thermal conductivity, whose value is fifty times higher than the healthy value (Table 3). Since the fault affects the whole pipe length, the temperature of the downstream node (20) decreases by 7.30 °C (see Table 4). As a result, the temperature of the node 20 reduces by 10.3 % with respect to the healthy condition (Fig. 6).

As highlighted in Fig. 7 and Table 4, the faulty pipe was successfully localized, as well as the fault type and magnitude. In fact, the diagnostic approach predicts a value of $x_{Rth,s}$ for pipe 19-20 equal to 0.0221. This is an extremely positive result since the expected $x_{Rth,s}$ is only slightly lower than the predicted value. Moreover, the health indices x_{Rth} of the other healthy pipes are always higher than 0.92,

in both the supply and return pipelines. Though such values are not very close to 1, they are not representative of an actual change of DHN health state.

Finally, the diagnostic approach finds out that the predicted $x_{Q,s}$, $x_{Q,r}$, $x_{Rp,s}$ and $x_{Rp,r}$ are equal to one.

Since all health indices are accurately calculated, all DHN variables are also accurately estimated. In fact, the mass flow rate of each pipe is exactly assessed, while the prediction errors of each DHN node are lower than 0.02 °C, and in the range from -16 Pa to 99 Pa. As a consequence, the R_{th} of the faulty pipe is accurately calculated.

Table 4 – Fault #1: expected *vs.* predicted values

	Expected value	Predicted value
Health index	$x_{Rth,s} = 0.0205$	$x_{Rth,s} = 0.0221$
R_{th} [K/W]	$3.70 \cdot 10^{-4}$	$3.98 \cdot 10^{-4}$
Effect on the downstream node	$T_{20}^* - T_{20} = 7.29966$ °C	$T_{20}^* - T_{20} = 7.29960$ °C
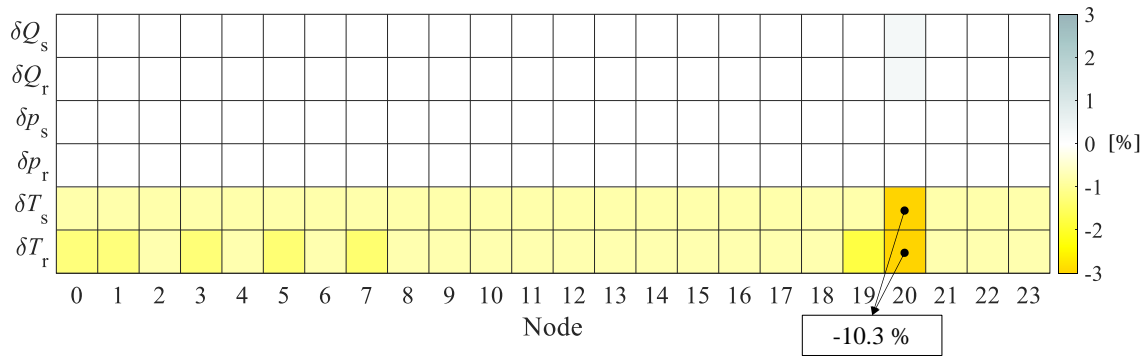
Figure 6 – Comparison between Fault #1 and the healthy scenario
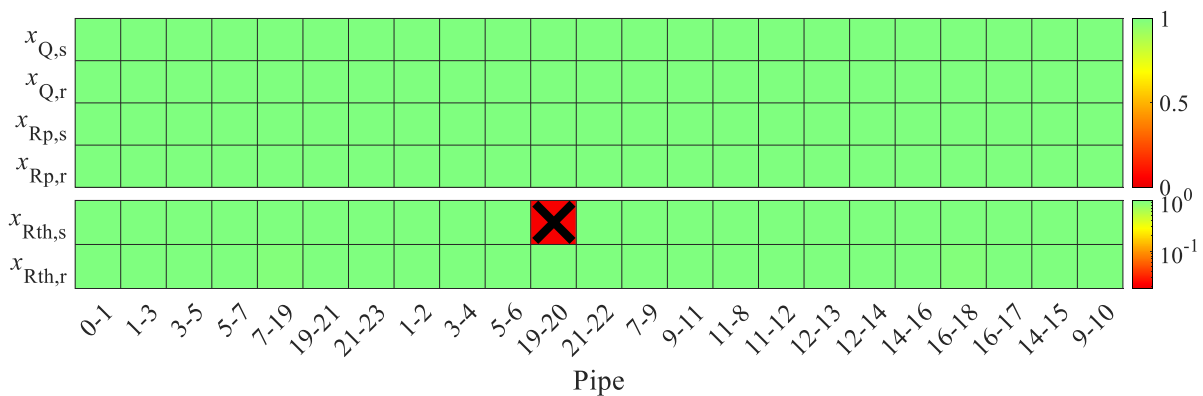
Figure 7 – Predicted health indices for Fault #1

Fault #2: anomalous pressure losses within pipe 19-20. In dataset #2, anomalous pressure losses occur along the pipe delimited by nodes 19 and 20, since the roughness is ten times higher (Table 3). As a result, the pressure of the downstream node decreases by

approximately 4 kPa (Table 5). Due to the fault #2, the mass flow rate that feeds the node 20 decreases by 2.10 % and its pressure is approximately 1 % lower than that in the healthy scenario (Fig. 8).

As can be noted from Fig. 9, the diagnostic approach correctly detects the faulty pipe, as well as the fault type and magnitude. In fact, the predicted $x_{Rp,s}$ is only slightly higher than the expected value (Table 5).

Table 5 – Fault #2: expected *vs.* predicted values

	Expected value	Predicted value
Health index	$x_{Rp,s} = 0.552$	$x_{Rp,s} = 0.556$
R_p [kg^{-1}·m^{-1}]	392.43	390.56
Effect on the downstream node	$p_{20}{}^* - p_{20} = 4.00$ kPa	$p_{20}{}^* - p_{20} = 4.00$ kPa
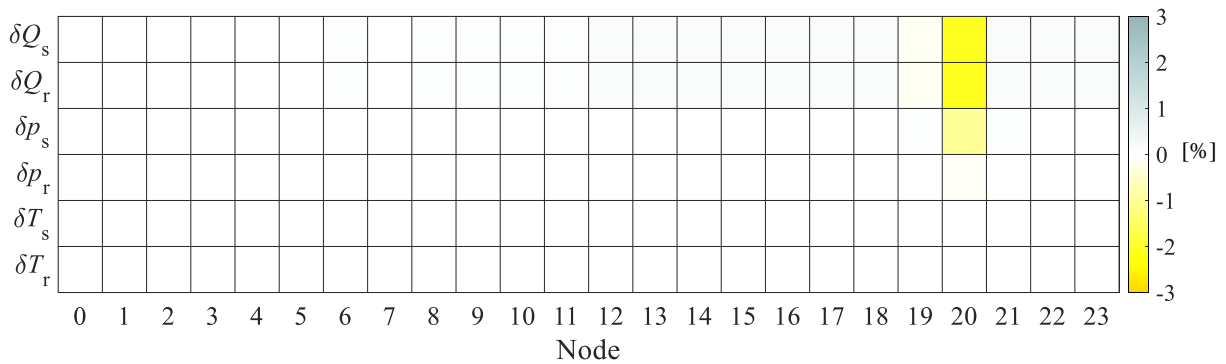
Figure 8 – Comparison between Fault #2 and the healthy scenario
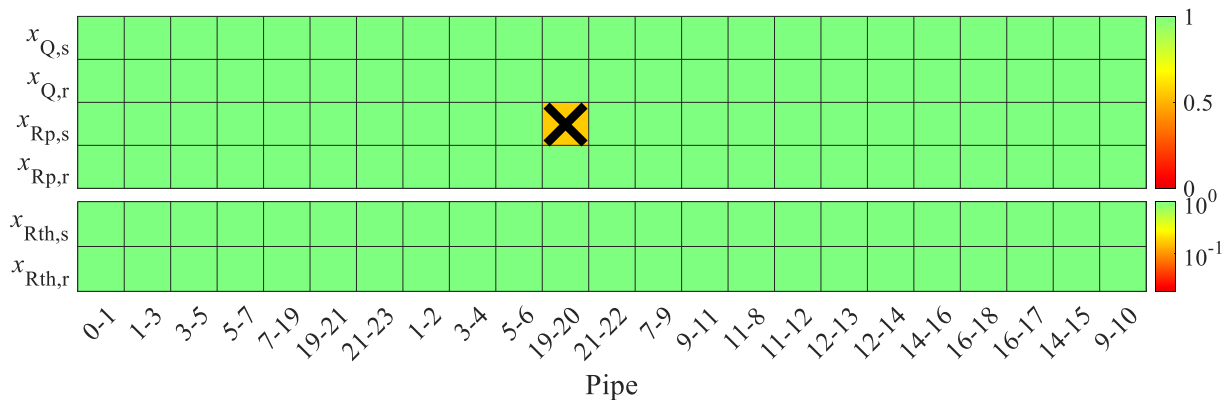
Figure 9 – Predicted health indices for Fault #2

The positive result is also confirmed by the fact that the health indices of the expected healthy pipes are found to be higher than 0.995. As a result, both the detection and identification tasks are successfully fulfilled. Based on the accurate diagnosis, all physical quantities are correctly predicted. In fact, the prediction error of the node temperatures is always lower than 0.002 °C.

Similarly, all node pressures are accurately predicted since the prediction error varies from -42 Pa (i.e., -0.013 %) to 92 Pa (i.e., 0.023 %).

Fault #3: anomalous pressure losses within pipe 12-14. In dataset #3, pipe 12-14 has a halved internal diameter for 10% of pipe length. As a consequence, the pressure of the node 14 decreases by 0.66 kPa with respect to the healthy condition (Table 6), which corresponds to an expected $x_{Rp,s}$ equal to 0.236.

As shown in Fig. 10, the mass flow rate that feeds nodes 14 through 18, i.e., the downstream nodes of the faulty pipe, is about 0.5 % lower than that in the healthy scenario, while their pressure reduces by 0.2 %.

Once again, the implanted fault is correctly detected and identified (Fig. 11). In fact, the predicted $x_{Rp,s}$ of the faulty pipe is by far the lowest health index, since it is roughly equal to 0.261, while the predicted health indices of the healthy pipes are always higher than 0.992. This is a significant result because the fault affects an intermediate pipe, whose upstream and downstream nodes are not included within the objective function (see Eqs. (6) and (7)).

As a result, the error of the predicted temperatures is the same as in Fault #2 (i.e., 0.002 %); instead, pressure errors are slightly higher, i.e., in the range from -87 Pa (-0.028 %) to 92 Pa (0.023 %).

Table 6 – Fault #3: expected *vs.* predicted values

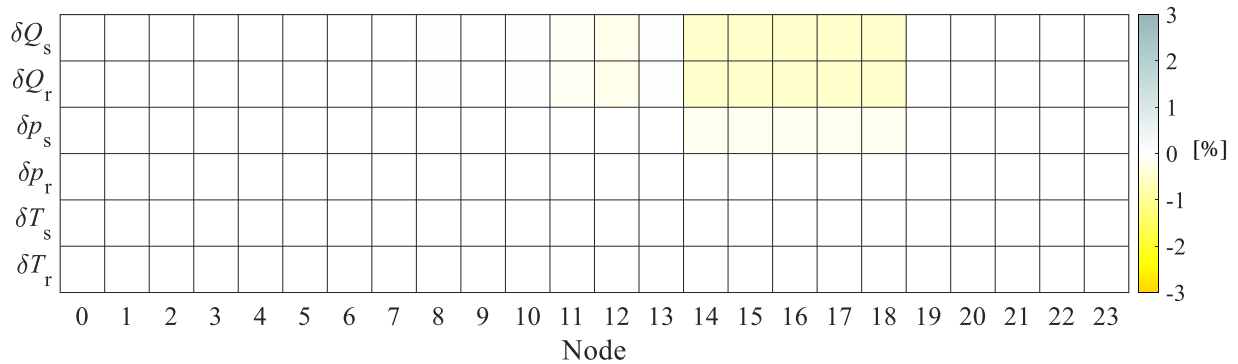|	Expected value	Predicted value
Health index	$x_{Rp,s} = 0.236$	$x_{Rp,s} = 0.261$
R_p [kg^{-1}·m^{-1}]	50.75	45.76
Effect on the downstream node	$p_{14}{}^* - p_{14} = 0.66$ kPa	$p_{14}{}^* - p_{14} = 0.65$ kPa

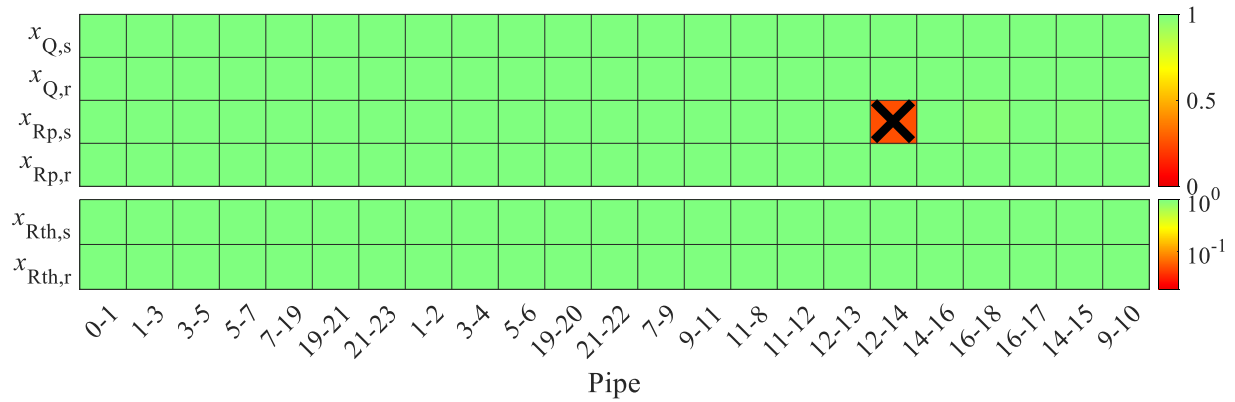**Figure 10** – Comparison between the Fault #3 and the healthy scenario

Figure 11 – Predicted health indices for Fault #3

Fault #4: leakage within pipe 11-12. In this case, 2.0 % of the water pumped out of the thermal power plant leaks; such a rate corresponds to 18.92 % of hot water passing through pipe 11-12. Thus, the expected $x_{Q,s}$ of the faulty pipe is equal to 0.811 (Table 7).

Table 7 – Fault #4: expected *vs.* predicted values

	Expected value	Predicted value
Health index	$x_{Q,s} = 0.811$	$x_{Q,s} = 0.915$
Effect on the downstream node	$Q = 8.57$ kg·s^{-1}	$Q = 9.98$ kg·s^{-1}

As shown in Fig. 12, the water leakage mainly affects the mass flow rate and the pressure of each node of the DHN. To counteract the effect of the water loss, the mass flow rate pumped out from the power plant has to be higher than that under the healthy scenario. Such a difference increases along those branches that connect the power plant to the faulty pipe. The maximum relative difference, i.e., 13.2 %, occurs at node 11, since it is the upstream node of the faulty pipe.
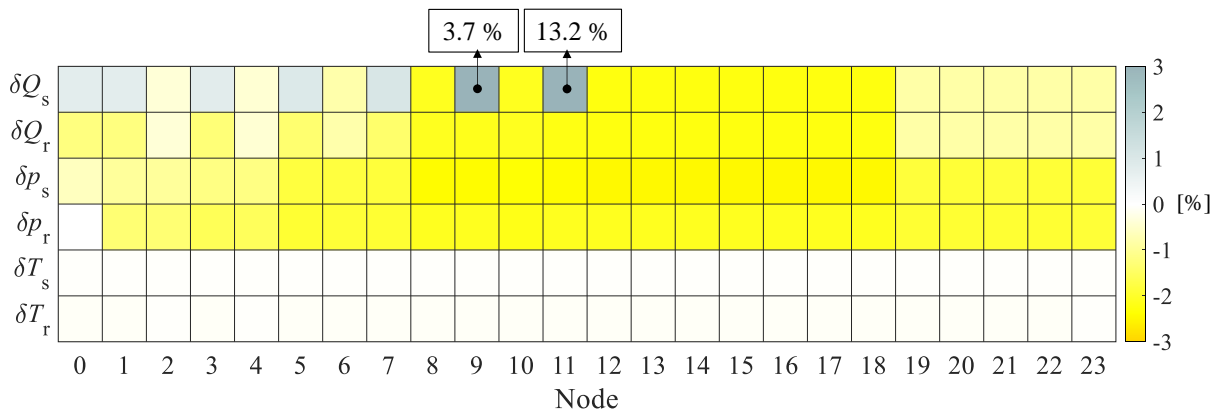

Figure 12 – Comparison between Fault #4 and the healthy scenario

As can be grasped from Figs. 13 and 14, the leakage significantly challenges the diagnostic approach. In fact, the fault occurs within a pipe whose upstream and downstream nodes are not included within the F_{ob} (see Eq. (7)).
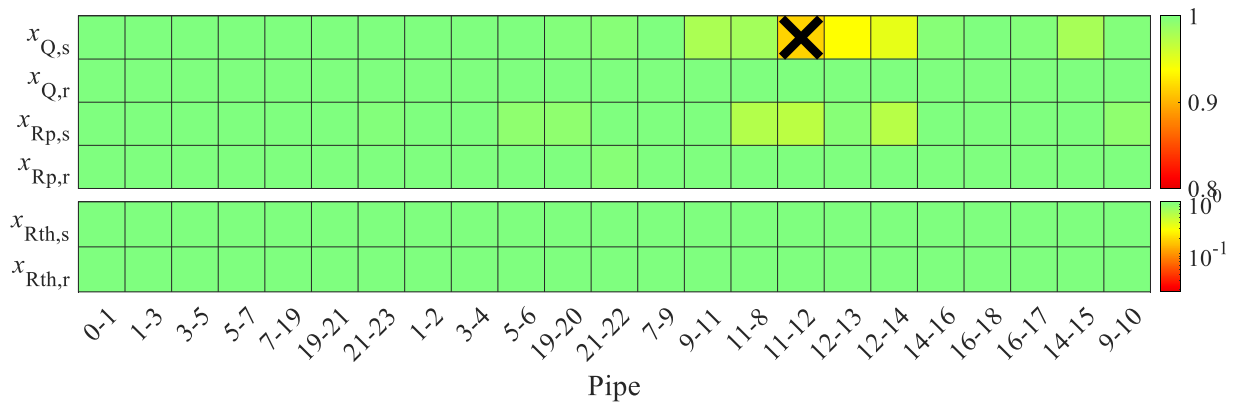

Figure 13 – Predicted health indices for Fault #4
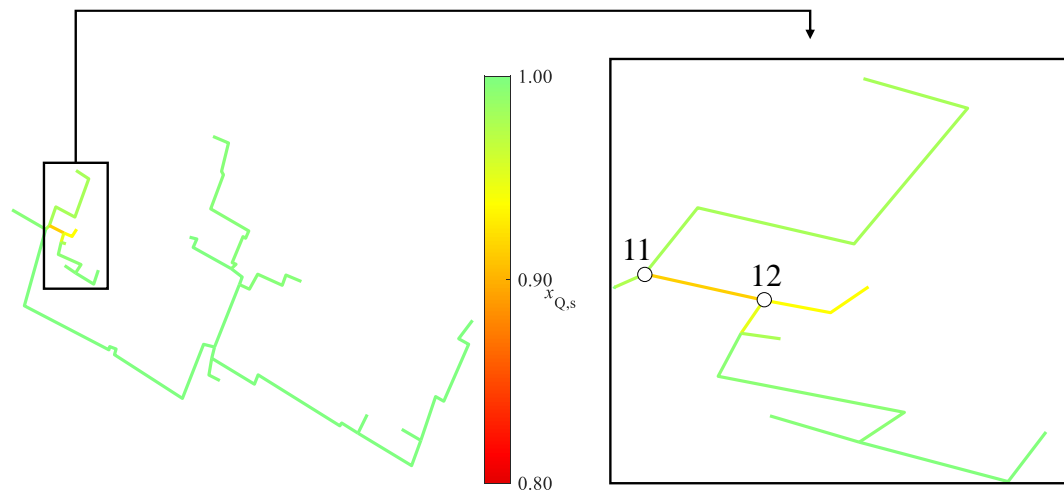

Figure 14 – Predicted $x_{Q,s}$ for Fault #4

Despite this, the diagnostic approach correctly detects the DHN zone where the fault occurs. In fact, the predicted $x_{Q,s}$ of pipe 11-12 is the lowest health index, though the diagnostic approach underestimates the fault magnitude, since the predicted $x_{Q,s}$ of the pipe 11-12 is found equal to 0.915. This outcome affects the DHN diagnosis in two different ways. First, the predicted $x_{Q,s}$ of a few healthy pipes is found lower than 1.00. More in detail, the predicted $x_{Q,s}$ of pipe 12-13 and 12-14 (see Fig. 14) is found equal to 0.94 and 0.95, respectively. This is an encouraging result, since the faulty pipe feeds 12-13 and 12-14; thus, the diagnosis made by the diagnostic approach is physically sound. In addition, the diagnostic approach also predicts that the $x_{Q,s}$ of the pipe that feeds the pipe 11-12 is roughly equal to 0.98. Second, because of this change, the mass flow rate that enters the pipe 11-12 is lower and the pressure losses are accordingly lower. Thus, the diagnostic approach estimates the predicted $x_{Rp,s}$ of the faulty pipe equal to 0.97 to artificially increase the

pressure losses along the pipe. It has to be mentioned that such a predicted value is the lowest x_{Rp} of all DHN health indices. Finally, the predicted values of x_{Rth} in both the supply and return pipelines are always higher than 0.99, as expected.

The correct diagnosis allows to correctly evaluate both the temperature and pressure of each node. In fact, the temperature prediction error is always lower than 0.001 °C, while the pressure prediction error is in the range from -227 Pa (i.e., -0.06 %) and 40 Pa (i.e., 0.01 %).

Fault #5: leakage within node 12. As mentioned in Section 2, the diagnostic approach has been developed for detecting and identifying faults that affect pipes. However, in this paper, the diagnostic approach is also tested to detect leakages that take place in a node.

In fact, in Fault #5, water is lost at the splitting junction node named 12, which is the downstream node of the pipe 11-12. As in Fault #4, 18.92 % of hot water passing through pipe 11-12 is lost (see Table 7) and the mass flow rate at node 11 is 13.2 % higher than that under the healthy condition (see Fig. 12). Thus, the expected health index is equal to 0.811. Thus, the diagnosis of Fault #4 and #5 can be directly compared.

As a general comment, the diagnostic approach correctly identifies the DHN zone in which the leakage occurs (Fig. 15), as well as the fault type. In fact, the lowest health indices are found in pipes 11-12, 12-14 and 12-13, whose predicted $x_{Q,s}$ are roughly equal to 0.90, 0.92 and 0.92, respectively. This is a positive outcome because 12 is the downstream node of pipe 11-12, while it is the upstream node of pipes 12-14 and 12-13 (Fig. 16).
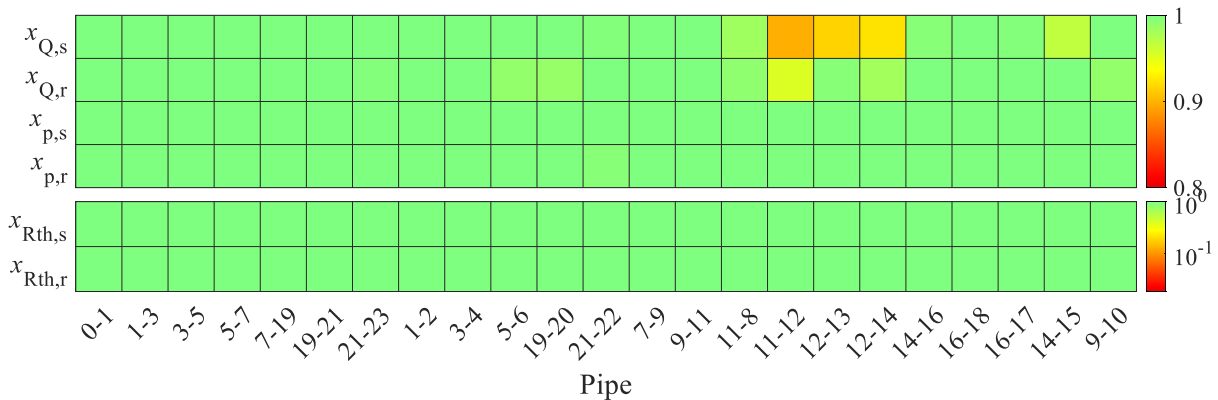

Figure 15 – Predicted health indices for Fault #5

Instead, in Fault #4, the health indices $x_{Q,s}$ of pipes 11-12, 12-14 and 12-13 are equal to 0.91, 0.94 and 0.95. Even though the diagnosis of two faulty scenarios is similar, in Fault #5 the predicted $x_{Q,s}$ of pipes 11-12, 12-14 and 12-13 are approximately the same, while slightly more scattered results are obtained in Fault #4. This result may be explained by considering that the fault occurs in two different ways and the diagnostic approach accordingly provides a slightly different response. In particular, the magnitude of Fault #5 is almost equally distributed among the pipes that are directly connected to the faulty node.

In Fault #5, the leakage is also confirmed by the fact that the predicted x_{Rth} and x_{Rp} are always higher than 0.99, with the exception of the pressure losses of pipes 11-12 and 12-14, in which $x_{Rp,s}$ is set equal to 0.95 and 0.98, respectively. As mentioned in the discussion about Fault #4, such a result can be explained by considering that the predicted flow rate passing through these pipes is lower than the expected value and thus the $x_{Rp,s}$ is found lower than one to artificially increase the pressure losses.

Therefore, the actual health state of the DHN is correctly assessed, by strengthening the capability of the diagnostic approach. Finally, prediction errors achieved for Fault #5 were of the same order of magnitude as the ones obtained for Fault #4.
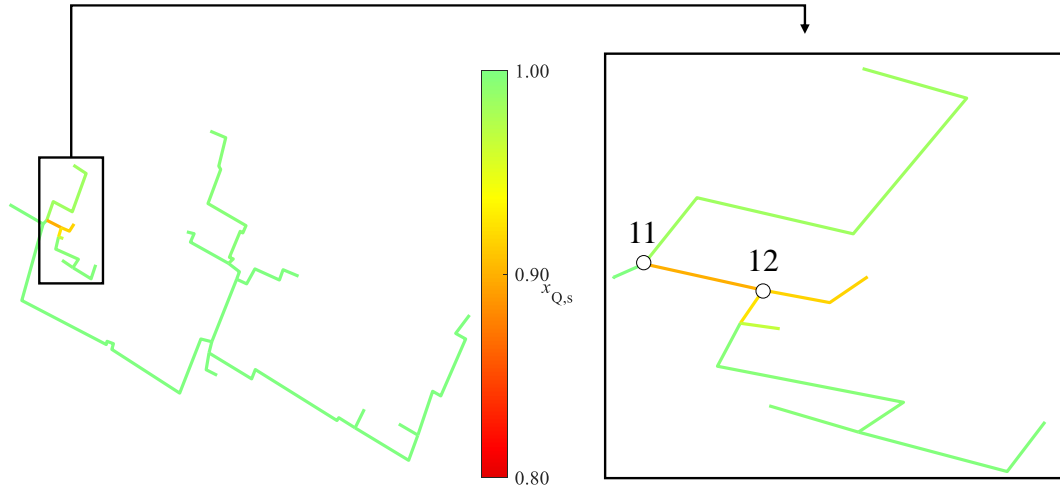

Figure 16 – Predicted $x_{Q,s}$ for Fault #5

4.2 Multiple faults

Fault #6: anomalous pressure and heat losses within pipe 12-14. Finally, the diagnostic approach is tested against two different fault types that affect pipe 12-14. In this analysis, the pipe internal diameter halved along 10 % of the pipe length, while the thermal conductivity of the whole insulating material is 20 W·m^{-1}·K^{-1} (Table 3).

Because of these two concurrent effects, the pressure of the downstream node, i.e., node 14, is 0.66 kPa lower than the pressure under healthy condition, while its temperature drop is slightly higher than 1 °C (Table 8).

Table 8 – Fault #6: expected *vs.* predicted values

	Expected value	Predicted value
Health indices	$x_{Rp,s} = 0.237$	$x_{Rp,s} = 0.262$
	$x_{Rth,s} = 0.039$	$x_{Rth,s} = 0.039$
R_p [kg^{-1}·m^{-1}]	50.75	45.73
R_{th} [K·W^{-1}]	3.53·10^{-3}	3.51·10^{-3}
Effect on the downstream node	$p_{14}^* - p_{14} = 0.66$ kPa	$p_{14}^* - p_{14} = 0.66$ kPa
	$T_{14}^* - T_{14} = 1.10$ °C	$T_{14}^* - T_{14} = 1.10$ °C

As can be grasped from Fig. 17, the faults mainly affect the mass flow rate and temperature of nodes 14 through 18, since their drops is approximately equal to 0.43 % and 1.6 %.

The diagnosis performed by the diagnostic approach is depicted in Fig. 18, which highlights that both faults are successfully detected and identified. In addition, fault magnitudes are accurately evaluated, since the predicted $x_{Rth,s}$ of pipe 12-14 is roughly equal to the

expected value, as well as the predicted $x_{Rp,s}$. This positive result is also confirmed by the fact that no water leakage is detected (i.e., all predicted x_Q values are found equal to 1) and the predicted x_{Rth} values do not highlight anomalous heat losses in the expected healthy pipes.

The accuracy of the diagnostic approach is also demonstrated by the negligible prediction error with which all DHN variables are calculated. In fact, temperature errors are in the range from -0.02 °C to 0.005 °C; in relative terms, they are always lower than 0.02 %. Similarly, the predicted pressures differ less than 0.03% (i.e., 95 Pa) from the expected values.
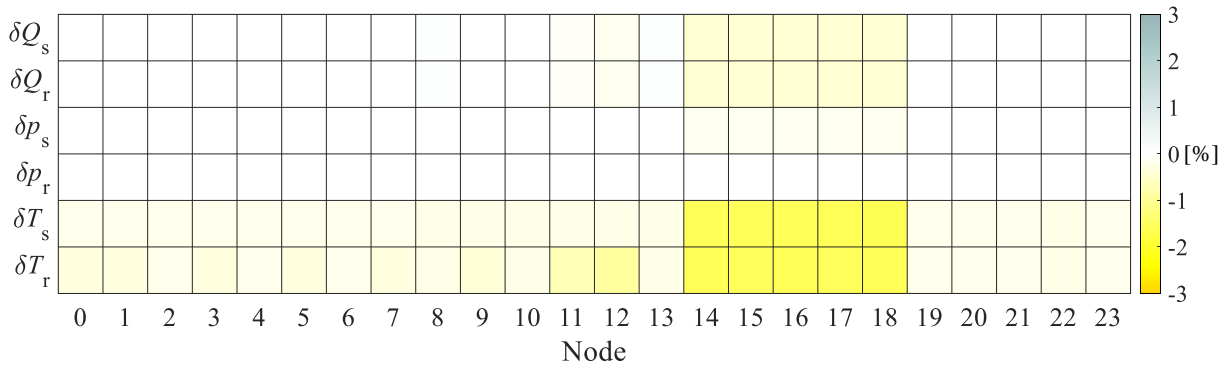

Figure 17 – Comparison between Fault #6 and the healthy scenario
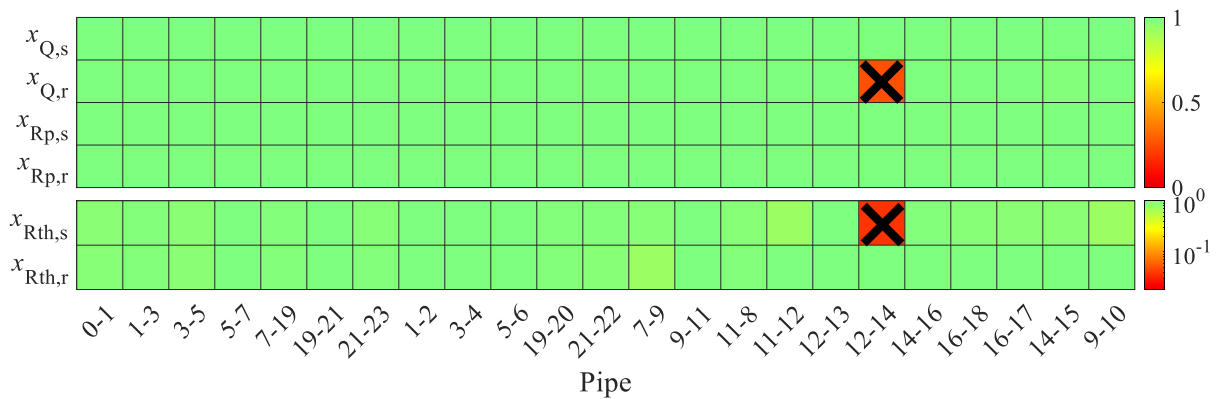

Figure 18 – Predicted health indices for Fault #6

Fault #7: anomalous pressure losses within pipe 12-14. Due to the anomalous pressure losses caused by the increase in the pipe roughness and decrease in the pipe internal diameter, the pressure of node 14 decreases by 1.46 kPa with respect to the healthy condition (Table 9). As a result, the expected $x_{Rp,s}$ is equal to 0.124. As mentioned in the discussion about Fault #3, the fault mainly affects the downstream nodes of the faulty pipe, i.e., nodes 14 through 18, since their mass flow rate and pressure are approximately 1 % and 0.4 % lower than the corresponding values under the healthy condition, respectively (Fig. 19).

Based on Table 9 and Fig. 20, both the detection and identification tasks are successfully performed, since the lowest predicted health index is assigned to 12-14 ($x_{Rp,s}$ equal to 0.131). Since the diagnostic approach slightly underestimates the pressure losses occurring in the faulty pipe, the health index $x_{RP,s}$ of the two downstream pipes is lower than one, i.e., 0.96 and 0.99.

	Expected value	Predicted value
Health index	$x_{\text{Rp,s}} = 0.124$	$x_{\text{Rp,s}} = 0.131$
R_p [kg^{-1}·m^{-1}]	96.73	91.61
Effect on the downstream node	p_{14}^* - $p_{14} = 1.46$ kPa	p_{14}^* - $p_{14} = 1.46$ kPa

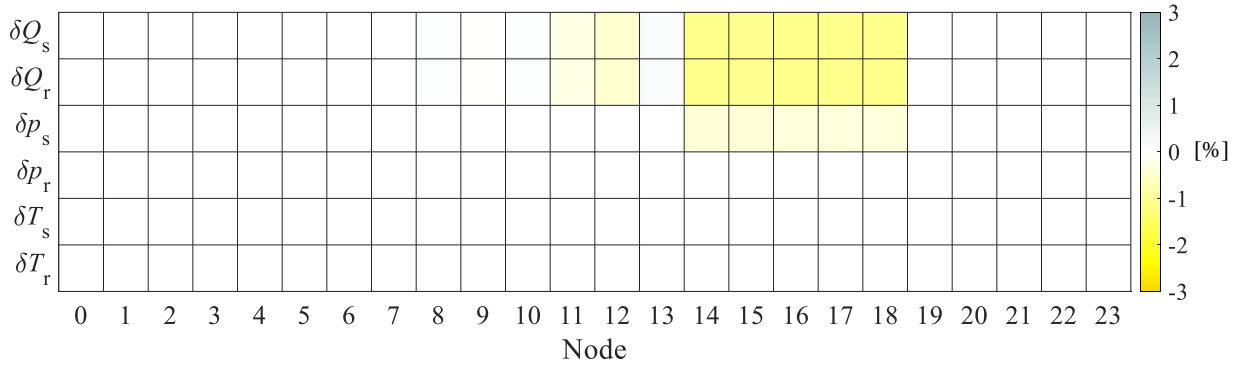**Table 9** – Fault #7: expected *vs.* predicted values

Figure 19 – Comparison between Fault #7 and the healthy scenario
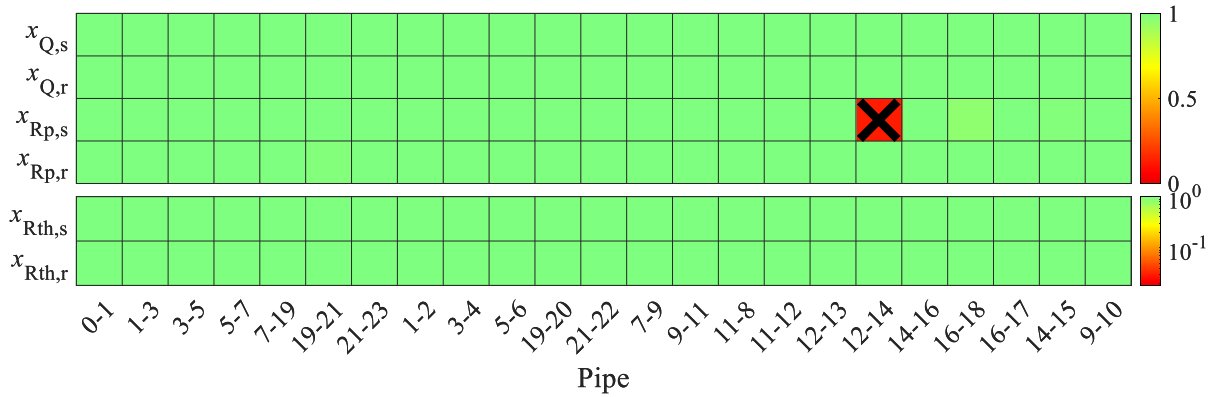

Figure 20 – Predicted health indices for Fault #7

Instead, the predicted $x_\text{Q,s}$ and $x_\text{Rth,s}$ are equal to one, by confirming that no leakage and no anomalous heat loss are detected in the supply pipeline; in the return pipeline, the predicted x_Rp and x_Rth are always higher than 0.98, thus confirming that no fault affects the return pipeline.

Based on the outstanding diagnostic capability, all DHN variables are correctly evaluated, with negligible prediction errors in the order of magnitude of 0.002 °C (i.e., 0.002 %) and in the range from -42 Pa (i.e., -0.013 %) to 92 Pa (i.e., 0.023 %).

5. CONCLUSIONS

The efficient operation of a District Heating Network (DHN) can be compromised by different faults that can be classified as water leakage, anomalous heat loss and pressure loss. Thus, diagnostic methodologies have to be developed and tuned to promptly detect the faulty pipes, thus preventing anomalous energy consumption and economic losses.

This goal was tackled by this study, which presented the development and validation of a novel diagnostic approach that detects and identifies three fault types, by also providing reliable health indices for each pipe of the DHN under analysis. In the proposed diagnostic approach, all health indices and variables of the DHN (i.e., mass flow rates, temperatures and pressures) are provided by coupling a DHN simulation model with an optimization algorithm that compares the calculated and measured DHN variables.

The novel diagnostic approach was validated by considering twenty-two faults that may hypothetically affect the DHN of the campus of the University of Parma. The measured DHN variables were generated by means of a model that acts as a digital twin of the DHN.

The proposed diagnostic approach was tested to detect and identify twenty-two faults, of which seven were investigated and thoroughly discussed in this paper to highlight the reliability and capability of the diagnostic approach. The seven faults included both single and multiple faults: single faults occurred when only one pipe was faulty, and the fault type was unique; conversely, multiple faults occurred because of multiple concurrent causes.

Based on the results, both single and multiple faults were accurately detected and identified. This is an extremely positive result, since the digital twin mimics the actual dynamic behavior of the real DHN, whereas the diagnostic model performs the DHN diagnosis under steady-state conditions.

The results also revealed that water leakages occurring within a pipe may challenge the novel diagnostic approach, but the DHN diagnosis was always physically sound. As a result, the detection and identification of the faulty zone were always guaranteed.

The reliability of the novel diagnostic approach was also proved since both the temperature and pressure of each node of the DHN were accurately calculated. In fact, the error between the temperatures simulated by the digital twin and the ones calculated by the diagnostic approach was usually lower than 0.02 °C (i.e., 0.02 %), while the pressure error was usually in the range from – 230 Pa (i.e., - 0.06 %) to 99 Pa (i.e., 0.030 %).

Finally, the novel diagnostic approach was checked to detect a water loss within a faulty node. Also in this case, the fault type was correctly identified, and the leakage was correctly split among the pipes connected to the faulty node. This all-in-all positive outcome, which allows the correct localization of the fault, can be explained by considering that the diagnostic approach accounts for losses of water occurring in a pipe, not in a node.

Based on these positive results, future works are planned to further test the robustness of the diagnostic methodology by using noisy simulated data, which mimic measurement uncertainty. Such analysis will be crucial in order to identify the required accuracy of the measurement devices to be installed. In the last step, the diagnostic approach will be tested by means of experimental data.

REFERENCES

[1] T. Tereshchenko, N. Nord, Importance of Increased Knowledge on Reliability of District Heating Pipes, 8th International Cold Climate HVAC 2015 Conference, CCHVAC 2015, Procedia Engineering 146 (2016), 415 – 423, http://doi.org/10.1016/j.proeng.2016.06.423.

[2] M. Sulzer, S. Werner, S. Mennel, M. Wetter, Vocabulary for the fourth generation of district heating and cooling, Smart Energy 1 (2021) 100003, https://doi.org/10.1016/j.segy.2021.100003.

[3] C. Mateu-Royo, S. Sawalha, A. Mota-Babiloni, J. Navarro-Esbrí, High temperature heat pump integration into district heating network, Energy Conversion and Management 210 (2020) 112719, https://doi.org/10.1016/j.enconman.2020.112719.

[4] D. Balic, D. Maljkovic, D. Loncar, Multi-criteria analysis of district heating system operation strategy, Energy Conversion and Management 144 (2017) 414-428, http://dx.doi.org/10.1016/j.enconman.2017.04.072.

[5] T.M Tveit, T. Savola, A. Gebremedhin, C.J. Fogelholm, Multi-period MINLP model for optimising operation and structural changes to CHP plants in district heating networks with long-term thermal storage, Energy Conversion and Management 50 (2009) 639-647, https://doi.org/10.1016/j.enconman.2008.10.010.

[6] N. Pardo García, G. Zubi, G. Pasaoglu, R. Dufo-Lopez, Photovoltaic thermal hybrid solar collector and district heating configurations for a Central European multi-family house, Energy Conversion and Management 148 (2017) 914-924, http://dx.doi.org/10.1016/j.enconman.2017.05.065.

[7] L.M.P. Ghilardi, A.F. Castelli, L. Moretti, M. Morini, E. Martelli, Co-optimization of multi-energy system operation, district heating/cooling network and thermal comfort management for buildings, Applied Energy 302 (2021) 117480, https://doi.org/10.1016/j.apenergy.2021.117480.

[8] M. Capone, E. Guelpa, G. Manco, V. Verda, Integration of storage and thermal demand response to unlock flexibility in district multi-energy systems, Energy 237 (2021) 121601, https://doi.org/10.1016/j.energy.2021.121601.

[9] N. Zimmerman, E. Dahlquist, K. Kyprianidis, Towards On-line Fault Detection and Diagnostics in District Heating Systems, The 8th International Conference on Applied Energy – ICAE2016, https://doi.org/10.1016/j.egypro.2017.03.567.

[10] R. Isermann, Model-based fault-detection and diagnosis – status and applications, Annual Reviews in Control 29 (2005) 71–85, https://doi.org/10.1016/j.arcontrol.2004.12.002.

[11] E. Guelpa, V. Verda, Automatic fouling detection in district heating substations: Methodology and tests, Applied Energy 258 (2020) 114059, https://doi.org/10.1016/j.apenergy.2019.114059.

[12] R. Kim, Y. Hong, Y. Choi, S. Yoon, System-level fouling detection of district heating substations using virtual-sensor-assisted building automation system, Energy 227 (2021) 120515, https://doi.org/10.1016/j.energy.2021.120515.

[13] P. Wang, P. Poovendran, K.B. Manokaran, Fault detection and control in integrated energy system using machine learning, Sustainable Energy Technologies and Assessments 47 (2021) 101366, https://doi.org/10.1016/j.seta.2021.101366.

[14] H.P. Lidén, B. Adl-Zarrabi, Development of a Non-destructive Testing Method for Assessing Thermal Status of District Heating Pipes, Journal of Nondestructive Evaluation (2020) 39:22, https://doi.org/10.1007/s10921-020-0667-5.

[15] P. Xue, Y. Jiang, Z. Zhou, X. Chen, X. Fang, X., J. Liu, Machine learning-based leakage fault detection for district heating Networks, Energy & Buildings 223 (2020), 110161 https://doi.org/10.1016/j.enbui ld.2020.110161.

[16] K. Hossain, F. Villebro, S. Forchhammer, UAV image analysis for leakage detection in district heating systems using machine learning, Pattern Recognition Letters 140 (2020) 158-164, https://doi.org/10.1016/j.patrec.2020.05.024.

[17] H. Wang, H. Meng, T. Zhu, New model for onsite heat loss state estimation of general district heating network with hourly measurements, Energy Conversion and Management 157 (2018) 71-85, https://doi.org/10.1016/j.enconman.2017.11.062.

[18] M. Li, W. Deng, K. Xiahou, T. Ji, Q. Wu, A Data-Driven Method for Fault Detection and Isolation of the Integrated Energy-Based District Heating System, IEEE Access, http://doi.org/10.1109/ACCESS.2020.2970273.

[19] S. Buffa, M. H. Fouladfar, G. Franchini, I. L. Gabarre, M. A. Chicote, Advanced Control and Fault Detection Strategies for District Heating and Cooling Systems—A Review, applied sciences 11 (2021), 455 Appl. Sci. 2021, 11, 455. https://doi.org/10.3390/app11010455.

[20] S. Månsson, P. O. J. Kallioniemi, M. Thern, T. Van Oevelen, K. Sernhed, Faults in district heating customer installations and ways to approach them: Experiences from Swedish utilities, Energy 180 (2019) 163-174, http://doi.org/10.1016/j.energy.2019.04.220.

[21] D. Hallberg, B. Stojanovic, J. Akander, Status, needs and possibilities for service life prediction and estimation of district heating, Structure and Infrastructure Engineering 8 (2012), 41-54, http://doi.org/10.1080/15732470903213740.

[22] S. Rimkevicius, A. Kaliatka, M. Valincius, G. Dundulis, R. Janulionis, A. Grybenas, I. Zutautaite, Development of approach for reliability assessment of pipeline network systems, Applied energy 94 (2012) 22-23, http://doi.org/10.1016/j.apenergy.2012.01.015.

[23] Zorc B, Kosec B, Kosec L, Nagode A. Analysis of hot water pipeline system leakage. Engineering Failure Analysis 2013;28:78-81. https://doi.org/10.1016/j.engfailanal.2012.10.001

[24] T.M. Walki, W.W Sharp, F.D.J Shields, Predicting internal roughness in water mains, Miscellaneous paper EL-88-2, US Army Engineer waterways experiment station, Vicksburg, Miss. (1988).

[25] M. Badami, A. Portoraro, Studio e caratterizzazione di reti termiche distribuite, Report RdS/2013/105, https://www.enea.it/it/Ricerca_sviluppo/documenti/ricerca-di-sistema-elettrico/risparmio-energia-settore-civile/2012/rds-2013-105.pdf (in Italian).

[26] Vega Am Yarahmadi N, Jakubowicz I. Determining the useful life of district heating pipes: Correlation between natural and accelerated ageing. Polymer Degradation and Stability 2020;175,109117. https://doi.org/10.1016/j.polymdegradstab.2020.109117

[27] A. M. Gusyachkin, L. S. Sabitov, A. M. Khakimova, A. R. Hayrullin, Effects of moisture content on thermal conductivity of thermal insulation materials, IOP Conf. Series: Materials Science and Engineering 570 (2019) 012029, http://doi.org/10.1088/1757-899X/570/1/012029.

[28] B. Rüger, D. Pierl, M. Guber, J. Yin, M. Baur, H. Eberhard, F. Klawonn, K. Michels, Online Leak Attribution to Exclusion Areas Prototype Application, 16th International Symposium on District Heating and Cooling, DHC2018, 9–12 September 2018, Hamburg, Germany, Energy Procedia 149 (2018), 575-584, http://doi.org/10.1016/j.egypro.2018.08.222.

[29] S. Zhou, Z. O'Neill, C. O'Neill, A review of leakage detection methods for district heating networks, Applied Thermal Engineering 137 (2018) 567-574, https://doi.org/10.1016/j.applthermaleng.2018.04.010.

[30] A. Kaliatka, M. Valincius, Modeling of pipe break accident in a district heating system using RELAP5 computer code, Energy 44 (2012) 813-819, https://doi.org/10.1016/j.energy.2012.05.011.

[31] Y. Zhong, Y. Xu, X. Wang, T. Jia, G. Xia, A. Ma, L. Zhang, Pipeline leakage detection for district heating systems using multisource data in mid- and high-latitude regions, ISPRS Journal of Photogrammetry and Remote Sensing 151 (2019) 207-222, https://doi.org/10.1016/j.isprsjprs.2019.02.021.

[32] M. Kane, J. Rolle, "Quantum networks": a new approach for representing a network and evaluating hydraulic and thermal losses in district heating/cooling systems, Proceedings of ECOS 2020 - the 33rd International Conference on Efficiency, Cost, Optimization, Simulation and environmental impact of energy systems June 29-July 3, 2020, Osaka, Japan.

[33] S. Chicherin, V. Mašatin, A. Siirde, A. Volkova, Method for Assessing Heat Loss in A District Heating Network with A Focus on the State of Insulation and Actual Demand for Useful Energy, Energies 2020, 13, 4505, https://doi.org/10.3390/en13174505.

[34] P. Lidén, B. Adl-Zarrabi, C.E. Hagentoft, Diagnostic Protocol for Thermal Performance of District Heating Pipes in Operation. Part 2: Estimation of Present Thermal Conductivity in Aged Pipe Insulation, Energies 2021, 14, 5302, https://doi.org/10.3390/en14175302.

[35] T. Fang, R. Lahdelma, State estimation of district heating network based on customer measurements, Applied Thermal Engineering 73 (2014) 1211-1221, http://dx.doi.org/10.1016/j.applthermaleng.2014.09.003.

[36] R. Bettocchi, P.R. Spina, Diagnosis of gas turbine operating conditions by means of the inverse cycle calculation, International Gas Turbine & Aeroengine Congress & Exhibition, Indianapolis, Indiana — June 7-June 10, 1999, 994T-185.

[37] R. Bettocchi, M. Pinelli, P.R. Spina, M. Venturini, S. Sebastianelli, 2001, "A System for Health State Determination of Natural Gas Compression Gas Turbines", Proc. ASME Turbo Expo 2001, June 4-7, New Orleans, Louisiana, USA, ASME Paper 2001-GT-223.

[38] M. Pinelli, M. Venturini, 2002, "Application of Methodologies to Evaluate the Health State of Gas Turbines in a Cogenerative Combined Cycle Power Plant", Proc. ASME Turbo Expo 2002, June 3-6, Amsterdam, The Netherlands, ASME Paper GT-2002-30248.

[39] M. Pinelli, P.R. Spina, M. Venturini, 2012, "Gas Turbine Health State Determination: Methodology Approach and Field Application", International Journal of Rotating Machinery, vol. 2012, Article ID 142173, 14 pages. https://doi.org/10.1155/2012/142173.

[40] L. Manservigi, H. Bahlawan, E. Losi, M. Morini, P.R. Spina, M. Venturini, A diagnostic approach for fault detection and identification in district heating networks, Energy 251 (2022) 123988, https://doi.org/10.1016/j.energy.2022.123988.

[41] A. De Lorenzi, A. Gambarott, M. Morini, M. Rossi, C. Saletti, Setup and testing of smart controllers for small-scale district heating networks: an integrated framework. Energy 2020;205:118054. https://doi.org/10.1016/j.energy.2020.118054

[42] M.A. Ancona, L. Branchini, A. De Lorenzi, A. De Pascale, A. Gambarotta, F. Melino, M. Morini, Application of different modeling approaches to a district heating network. AIP Conference Proceedings 2019; 2191, 020009. https://doi.org/10.1063/1.5138742.

[43] S. Månsson, I. Lundholm Benzi, M. Thern, R. Salenbien, K. Sernhed, P.O. Johansson Kallioniem, A taxonomy for labeling deviations in district heating customer data. Smart Energy 2021;2,100020.

[44] M. Pipiciello, M. Caldera, M. Cozzini, M.A. Ancona, F. Melino, B. Di Pietra, Experimental characterization of a prototype of bidirectional substation for district heating with thermal prosumers, Energy 223 (2021) 120036, https://doi.org/10.1016/j.energy.2021.120036.

[45] Matlab release 2020a: https://it.mathworks.com.